1.D.1 *Nuclear Physics* **A243** (1975) 507–518; © *North-Holland Publishing Co., Amsterdam*
Not to be reproduced by photoprint or microfilm without written permission from the publisher

NUCLEAR RESPONSE IN THE CONTINUUM †

S. SHLOMO and G. BERTSCH
Department of Physics and Cyclotron Laboratory, Michigan State University, East Lansing, Michigan 48824

Received 10 December 1974
(Revised 27 January 1975)

Abstract: Continuum effects may be easily treated in the RPA particle-hole theory of excitations, if the calculation is done with the response function formalism. We apply the theory to the low multipolarities in ^{16}O, ^{40}Ca, and ^{208}Pb. We confirm that the width of the giant dipole state in light nuclei is accounted for by the continuum. In heavy nuclei the dipole decay width is relatively small. The giant quadrupole state is predicted to be much narrower than the dipole since it is concentrated in a single state. The $3\hbar\omega$ octupole state is quite spread out in light nuclei, but has a width of only 1 MeV in ^{208}Pb.

1. Introduction

Much attention has been devoted recently to nuclear excitations in the region of 10–40 MeV excitation, both experimentally [1–5]) and theoretically [6, 7]). The main object is to see whether other resonances besides the well-known giant dipole exist and are localized. The RPA theory [6, 7]) works surprisingly well in reproducing the position and strengths of isoscalar excitations of low multipolarity. These models are not able to predict the width of the states, because no mixing is allowed with configurations more complex than 1p-1h, and also the states have been treated as discrete even in the continuum.

Very recently the calculations of ref. [7]) have been extended to treat the continuum [ref. [8])] based on the method of Birkholz [9]); in this work we report a simple generalization of the method of ref. [6]) to treat the continuum. We first describe the method and then present some sample strength function calculations.

2. Theory

To derive our method we make use of the results and notation of ref. [6]). The response of the system to an external field described by the single-particle operator F is given by

$$\sum_n |\langle 0|F|n\rangle|^2 \delta(E-E_n) = \frac{1}{\pi} \operatorname{Im} \int \mathrm{d}r\, \mathrm{d}r' F(r) F(r') G(r, r', E), \tag{1}$$

where G is the particle-hole Green function. In RPA theory the Green function is

† Supported by the National Science Foundation.

given by

$$G^{\mathrm{RPA}} = G^{(0)} \left(1 - \frac{\delta V}{\delta \rho} G^{(0)}\right)^{-1}, \tag{2}$$

where V is the Hartree-Fock potential, having a functional dependence on ρ, the density. The unperturbed Green function $G^{(0)}$ is given in terms of the Hartree-Fock Hamiltonian H_0, its occupied eigenstates ϕ_h, and the associated eigenenergies ε_h, as

$$G^{(0)}(r_1, r_2, \omega) = -\sum_h \phi_h(r_1) \left(\frac{1}{H_0 - \varepsilon_h - \omega} + \frac{1}{H_0 - \varepsilon_h + \omega}\right) \phi_h(r_2). \tag{3}$$

The sum in eq. (3) is on the occupied states; $(H_0 - E)^{-1}$ is the Hartree-Fock Green function for a single particle propagated from r_2 to r_1. Note that eqs. (2) and (3) are operator equations in coordinate space; we represent them as matrix equations on a mesh in coordinate space. If H_0 possesses only a discrete spectrum, then the single-particle Green function is evaluated in coordinate space as

$$\left(\frac{1}{H_0 - E}\right)_{r_1 r_2} = \sum_p \phi_p(r_1) \frac{1}{\varepsilon_p - E} \phi_p(r_2). \tag{4}$$

Substituting (4) into (3), we obtain a double sum. The sum over p can be restricted to unoccupied states, since the two terms in eq. (3) will cancel contributions from occupied orbits. The RPA theory was solved in this form in ref. [6]).

The essential trick for exact treatment of the continuum is to write the single-particle Green function with the well-known representation [10])

$$g_{lj}(r_1, r_2, E) = \frac{1}{H_0 - E} = -\frac{2m}{\hbar^2} u_{lj}(r_<) v_{lj}(r_>)/W, \tag{5}$$

instead of with eq. (4). Here u_{lj} is the regular solution of the Hartree-Fock Hamiltonian for the lj partial wave, and v_{lj} is an irregular solution. In eq. (5), $r_<$ and $r_>$ denote the lesser and the greater of r_1 and r_2, respectively. The irregular solution is determined by the boundary condition at ∞. For negative energies, this is

$$v(r) \sim \exp[-\sqrt{2mE/\hbar^2}\, r], \qquad r \to \infty. \tag{6}$$

For positive energies, $v(r)$ describes an outgoing wave asymptotically,

$$v(r) \sim \exp[i\sqrt{2mE/\hbar^2}\, r], \qquad r \to \infty. \tag{7}$$

The normalization of the Green function is determined by the Wronskian, W, of the two solutions,

$$W = u \frac{\mathrm{d}v}{\mathrm{d}r} - v \frac{\mathrm{d}u}{\mathrm{d}r}. \tag{8}$$

Using eqs. (1)–(3), and (5), we calculate the finite imaginary part of the response as a function of energy, and thereby obtain the broadening of the discrete states. Of course,

below threshold, there is no imaginary part to the response. It does have poles lying on the real axis, so positions and strengths of states can still be determined if necessary. When states are isolated and decay by different channels than they are formed, the method easily reduces to the standard golden rule for the widths. (This is shown in the appendix.)

It is important to emphasize that the single-particle Green function, eq. (5) contains the entire spectrum of H_0. The Pauli-violating transitions from occupied to occupied orbits are cancelled with the two terms in eq. (3), but this only occurs, numerically in RPA. In the TDA model, made by omitting the second term in (3), there is no cancellation and the poles from occupied states must be explicitly subtracted out of g_{lj}.

In practical terms, this theory is most nearly equivalent to the continuum theory of Buck and Hill [11]). These authors developed a fast method for calculating the continuum which relies on zero-range interactions. Our method is also fast, and since it uses a local particle-hole Green function, it also relies on zero-range exchange interactions. Our original treatment of the Green function was general enough to include some non-locality [6]), but in fact here we only use δ-function interactions. Also, for simplicity, we shall use a Woods-Saxon potential instead of a Hartree-Fock well to generate g_{lj} and $G^{(0)}$.

3. Results

Before displaying the results, some numerical remarks are in order. First, the numerical cancellation of the Pauli-violating transitions requires that the same numerical procedures be used to calculate the hole orbits and to calculate Green functions. Failure to do these initially gave us double poles and peculiar-looking fine structure, reminiscent of the numerical difficulties encountered in the eigenchannel method [12]).

To start the integration of the irregular function v, we use the prescription of Bloch *et al.* [13]) at a radius of 15–20 fm. The numerical integration is done in double precision with a mesh size not greater than 0.1 fm. As found previously [6]), the mesh for the $G^{(0)}$ matrix can be quite coarse (1 fm) and still yield an accuracy better than 5 %. As a check of the method and our computer code we have repeated the calculation of Buck and Hill [11]) for the giant dipole in ^{16}O. Using their interaction and the single-particle potential wells we have reproduced, in the TDA model, their results.

We first consider the isoscalar response of the nuclei. For simplicity, we used a state-independent Woods-Saxon potential which includes central, spin-orbit, symmetry and Coulomb potentials:

$$V(r) = \left(1-0.67\frac{N-Z}{A}\tau_z\right)\left(V_0 f(r)+V_{\text{s.o.}}\boldsymbol{\sigma}\cdot\boldsymbol{l}\frac{1}{r}\frac{\mathrm{d}}{\mathrm{d}r}f(r)\right)+\tfrac{1}{2}(1-\tau_z)V_{\text{Coul}}(r), \quad (9)$$

TABLE 1

Experimental and calculated single-particle energies (in MeV) for ^{16}O, ^{40}Ca, ^{208}Pb

Orbit		Neutron			Proton		
		exp.	local	non-local	exp.	local	non-local
^{16}O	$1s_{\frac{1}{2}}$		35.73	32.88	40 ± 8	31.86	27.62
	$1p_{\frac{3}{2}}$	21.8	20.34	21.81	18.4	16.79	18.45
	$1p_{\frac{1}{2}}$	15.7	15.25	15.66	12.1	11.72	12.12
	$1d_{\frac{5}{2}}$	4.14	5.47	4.14	0.60	2.34	0.58
	$2s_{\frac{1}{2}}$	3.27	3.89	3.28	0.10	1.13	0.11
	$1d_{\frac{3}{2}}$	−0.94	−1.25	−0.94		−4.60	−4.60
^{40}Ca	$1s_{\frac{1}{2}}$		43.63	43.51	50 ± 11	35.37	35.48
	$1p_{\frac{3}{2}}$		32.68	32.07		24.85	23.32
	$1p_{\frac{1}{2}}$		30.14	29.31	34 ± 6	22.26	20.49
	$1d_{\frac{5}{2}}$		20.98	21.32		13.59	14.03
	$2s_{\frac{1}{2}}$	18.1	17.04	18.14	10.9	9.67	10.94
	$1d_{\frac{3}{2}}$	15.6	15.89	15.69	8.3	8.46	8.33
	$1f_{\frac{7}{2}}$	8.32	8.92	8.33	1.4	2.02	1.38
	$2p_{\frac{3}{2}}$	6.2	5.65	6.21		−0.77	−0.77
	$2p_{\frac{1}{2}}$		3.50	3.70		−3.00	−2.67
	$1f_{\frac{5}{2}}$		1.43	1.74		−5.20	−4.82
^{208}Pb	$1s_{\frac{1}{2}}$		43.20	43.06		36.28	34.35
	$1p_{\frac{3}{2}}$		38.84	37.35		32.48	31.68
	$1p_{\frac{1}{2}}$		38.49	36.99		31.97	31.16
	$1d_{\frac{5}{2}}$		33.70	33.88		27.68	25.97
	$1d_{\frac{3}{2}}$		32.83	33.24		26.49	25.07
	$2s_{\frac{1}{2}}$		31.41	32.08		24.38	23.40
	$1f_{\frac{7}{2}}$		27.91	26.49		22.09	21.02
	$1f_{\frac{5}{2}}$		26.27	25.18		19.94	19.16
	$2p_{\frac{3}{2}}$		24.53	24.06		17.51	17.74
	$2p_{\frac{1}{2}}$		23.83	23.35		16.64	16.86
	$1g_{\frac{9}{2}}$		21.55	21.97	15.43	15.83	15.44
	$1g_{\frac{7}{2}}$		18.91	19.73	11.43	12.44	11.43
	$2d_{\frac{5}{2}}$		17.33	18.41	9.70	10.27	9.70
	$1h_{\frac{11}{2}}$		14.70	15.20	9.37	8.99	9.39
	$2d_{\frac{3}{2}}$		15.95	17.36	8.38	8.53	8.38
	$3s_{\frac{1}{2}}$		15.51	17.00	8.03	7.86	8.03
	$1h_{\frac{9}{2}}$	10.85	10.87	10.85	3.77	4.11	3.78
	$2f_{\frac{7}{2}}$	9.72	9.98	9.72	2.87	2.75	2.87
	$1i_{\frac{13}{2}}$	9.01	7.45	9.04	2.16	1.66	2.17
	$3p_{\frac{3}{2}}$	8.27	7.83	8.28	0.95	−0.27	0.95
	$2f_{\frac{5}{2}}$	7.95	7.84	7.96	0.47	−0.01	0.47
	$3p_{\frac{1}{2}}$	7.38	7.00	7.40		−1.37	−0.19
	$2g_{\frac{9}{2}}$	3.94	2.70	3.94			
	$1i_{\frac{13}{2}}$	3.15	2.28	3.15			
	$1j_{\frac{15}{2}}$	2.53	−0.13	2.53			
	$3d_{\frac{5}{2}}$	2.36	1.08	2.37			
	$4s_{\frac{1}{2}}$	1.91	0.73	1.92			
	$2g_{\frac{7}{2}}$	1.45	−0.03	1.44			
	$3d_{\frac{3}{2}}$	1.42	0.10	1.43			

The experimental values are those given in ref. [14]). Note that the local Woods-Saxon wells are used for giant resonances of multipoles $L \geqq 2$, whereas the non-locals are used in the calculation of the cross section for the giant dipoles.

where

$$f(r) = [1+\exp((r-R)/a)]^{-1}, \quad \text{with } a = 0.65\,\text{fm},$$

$$R = 1.20(A-1)^{\frac{1}{3}}\,\text{fm}, \qquad V_{\text{s.o.}} = 15\,\text{MeV}\cdot\text{fm}^2.$$

The Coulomb potential $V_{\text{Coul}}(r)$ is that of a uniform charge distribution with the empirical rms radius. The potential depth, V_0, is adjusted to give a reasonable fit to the separation energies of the least bound states [14]) ($-V_0 = 58$, 57 and 55.5 MeV for ^{16}O, ^{40}Ca and ^{208}Pb respectively). Note that in these model calculations, in order to get reasonable separations between occupied and unoccupied levels, we use potential wells with radii ($R = 1.20(A-1)^{\frac{1}{3}}$fm) that are smaller by $\approx 10\,\%$ than those commonly used. The single-particle energies for these local Woods-Saxon potentials are given in table 1. The interaction is of the Skyrme form [14]), with $t_0 = -1100$, $t_3 = 16000$, and $x = 0.5$ (no velocity dependence), neglecting terms with the σ-operator in the p-h interaction. With these parameters of the Skyrme force, the Hartree-Fock single-particle potentials obtained are in reasonable agreement with the Woods-Saxon potentials used in the calculation. To make the interaction self-consistent, we adjusted its strength to place the spurious state at zero energy, as done in ref. [6]). This is quite important, since the position of the quadrupole state is quite sensitive to the model if self-consistency is not enforced. With self-consistency, the position of the giant quadrupole is not very sensitive to the particle-hole excitation energies.

The response to the γ-field of multipolarity L is obtained from the single-particle operator $F = \sum e_i r_i^L Y^L$ with the effective charges [15])

$$e_{\text{p}} = ((A-1)/A)^L + (-1)^L(Z-1)/A^L,$$
$$e_{\text{n}} = (-1)^L Z/A^L. \tag{10}$$

This takes into account the recoil effect of the nucleus. We use an n-p formalism, and thus include the isoscalar as well as the isovector component of the response.

In figs. 1–3 we display the quadrupole response of the nuclei considered and in figs. 4–6 the octupole response is shown. The strength is given in single-particle units (s.p.u.),

$$\text{s.p.u.} = e^2\,\frac{2L+1}{4\pi}\left[\frac{3}{3+L}(1.2A^{\frac{1}{3}})^L\right]^2. \tag{11}$$

The isoscalar "giant quadrupole" state is at $60/A^{\frac{1}{3}}$ MeV; it appears as a single prominent peak, not significantly broadened by the decay widths. In fact, this narrowness could have been easily deduced to within a factor of two by the standard R-matrix estimates of single-particle widths and penetrabilities. Note also that the upper part of the response is due to isovector excitations.

The $L = 3$ strength functions, shown in figs. 4–6 do not show the strong $1\hbar\omega$ collective states since these are below threshold. The response function for an isolated

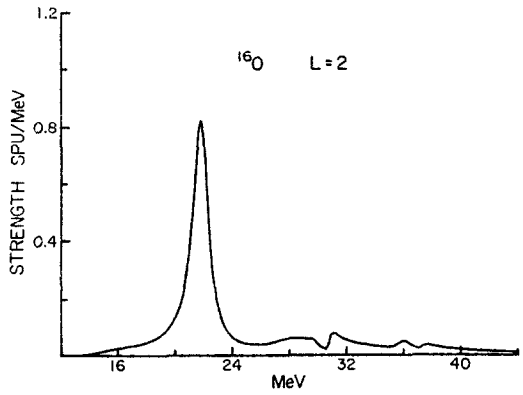

Fig. 1. The $L = 2$ response for γ-absorption in ^{16}O obtained in the RPA model. The strength is given in s.p.u./MeV. For details of the calculation see text.

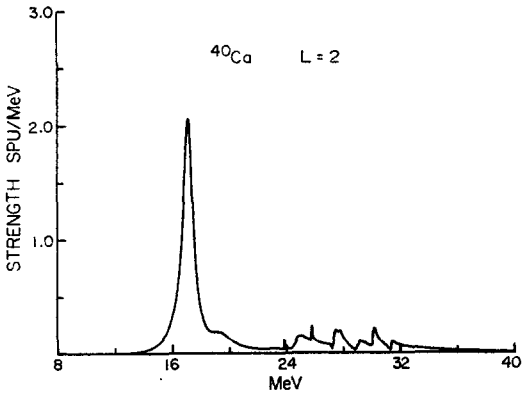

Fig. 2. Same as fig. 1 for ^{40}Ca.

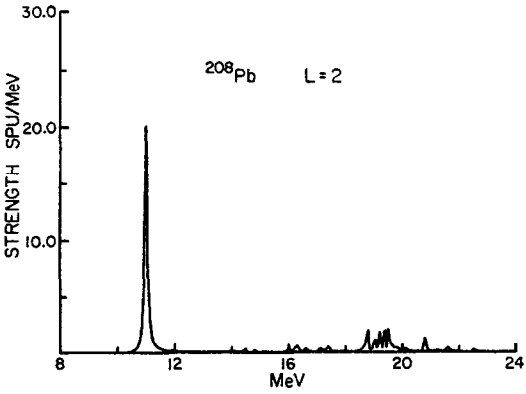

Fig. 3. Same as fig. 1 for ^{208}Pb.

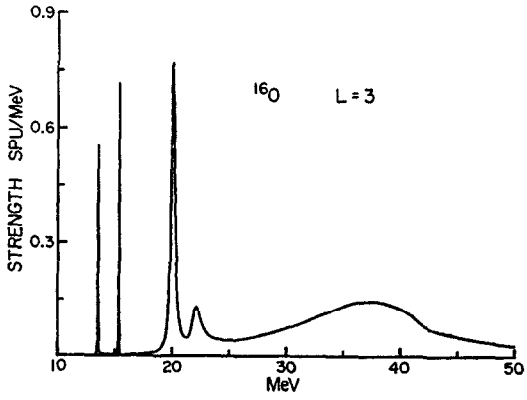

Fig. 4. Same as fig. 1 for $L = 3$ ^{16}O.

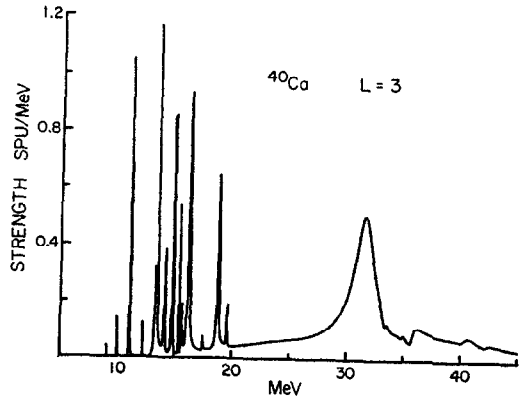

Fig. 5. Same as fig. 1 for $L = 3$ ^{40}Ca.

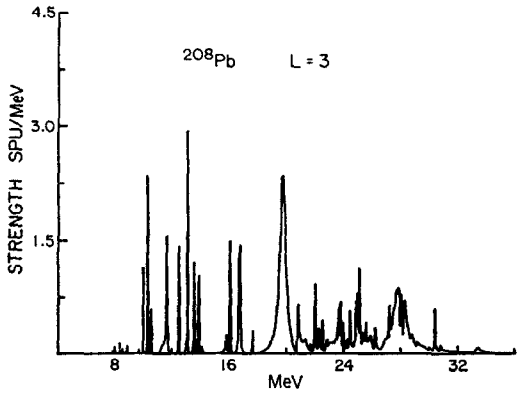

Fig. 6. Same as fig. 1 for $L = 3$ ^{208}Pb.

state at energy E_r can be written as

$$\langle FGF \rangle = \frac{S}{E - E_r + i\varepsilon}.$$

Using (2) we find that the transition rate is given by $-S$ (S is the residue of the pole). For a state below threshold, $\langle FGF \rangle$ is real. So the position of the level and the transition rate can be obtained by examining the energy dependence of the response function $\langle FGF \rangle$. We find that the low-lying octupole states in ^{16}O, ^{40}Ca and ^{208}Pb are located, in our model calculation, at 7.00, 3.53 and 2.94 MeV, in good agreement with the experimental values [6]) of 6.13, 3.74 and 2.61 MeV, respectively. We note that the present calculated values agree quite well and with those obtained in ref. [6]) using the interaction Skyrme I. However, the transition rates obtained here are smaller by a factor of 2–4 than those calculated in ref. [6]). This is mainly due to the fact that, in our calculations, the rms radii of the charge distributions are smaller by $\approx$ 10 % than the experimental values [and the results of ref. [6])]. This has a significant effect on the transition rates for high multipoles such as octupole (note that $(1.1)^6 = 1.77$). Excellent agreement with the values of ref. [6]) was obtained using $R = 1.35(A-1)^{\frac{1}{3}}$ fm and $a = 0.70$ fm for the parameters of the Woods-Saxon wells of ^{16}O and ^{40}Ca. With these parameters the calculated rms radii agree with experiment. As a consistency check of our model calculation we also mention here that the transition rates for the low-lying octupole states are enhanced by more than an order of magnitude as compared to typical single-particle transition rates obtained from the free response $\langle FG^0F \rangle$.

From fig. 6 we find that the $3\hbar\omega$ octupole is located at 19 MeV in ^{208}Pb and is fairly narrow. This is in agreement with the electron scattering results of Nagao *et al.* [2]). For the lighter nuclei this $3\hbar\omega$ state becomes broader and in ^{16}O it is no longer recognizable. Again, higher energy portions of the strength function are due to the isovector component.

Finally, to get an idea where the RPA theory reduces to the independent particle model, we display in fig. 7 the $L = 4$ strength in ^{16}O. Here the curve is very smooth, and enhanced only by a factor of two above the free response obtained with $G^{(0)}$.

Next we turn to the isovector dipole strength, which of course is the only multipole known at all well experimentally. Our calculations along the lines described for the isoscalar modes gave much too low a position for the dipole state. This is certainly due to the neglect of the velocity dependence of the interaction Hamiltonian. To get an improvement in the dipole response, the following changes were made.

First, the velocity dependence spreads out the single-particle spectrum, increasing the particle-hole excitation energies. This was accomplished by allowing the Woods-Saxon well to be state-dependent, and fitting the separation energy of bound and unbound orbits [14]). The form (9) is adopted with $R = 1.25(A-1)^{\frac{1}{3}}$, and V_0 and $V_{s.o.}$ are assumed to depend on τ_z and the orbital angular momentum l. The single-particle energies for these non-local potential wells are given in table 1.

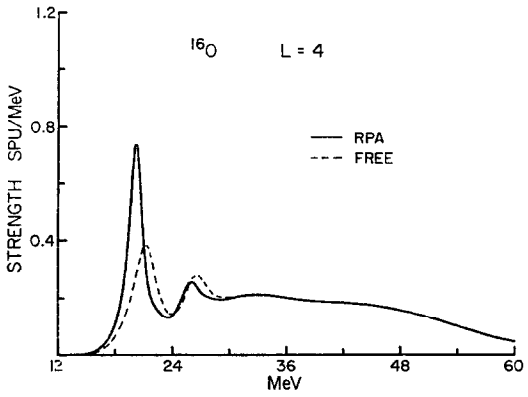

Fig. 7. Same as fig. 1 for $L = 4$ in ^{16}O. The solid curve is the perturbed response and the dashed curve is the free response obtained using $G^{(0)}$.

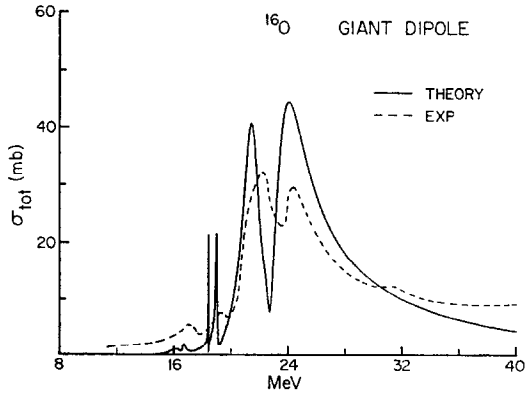

Fig. 8. Total cross section $(\gamma, p)+(\gamma, n)$ in mb for the giant dipole in ^{16}O obtained in the TDA model (solid curve) as compared to experimental results (dashed curve) [ref. [18])]. For details of the calculation see text.

Second, the velocity dependence of the interaction suppresses the backward-going amplitude in RPA relative to the forward-going amplitude. We therefore used TDA instead of RPA. Also, we used the Skyrme I interaction with the local treatment of velocity dependence given in ref. [6]). We include the interaction in the τ and $\tau\sigma$ channels (in the p-h representation).

The results for ^{16}O, ^{40}Ca and ^{208}Pb are shown in figs. 8–10. The location of the peak depends quite strongly on the single-particle excitation energies; a l-independent Woods-Saxon well yields an ^{16}O dipole state 4 MeV lower than that shown.

In ^{40}Ca and ^{208}Pb, the strength is distributed over several relatively sharp peaks of comparable intensity. This seems to depend on the relative positions of the $T = 0$, $S = 0$ strength with respect to the $T = 0$, $S = 1$ strength, which are mixed by the one-body spin-orbit potential. With a weaker interaction, the strengths are split far

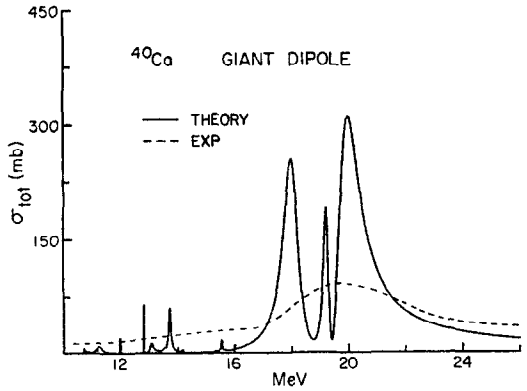

Fig. 9. Same as fig. 8 for ^{40}Ca. Experimental data are from ref. [18]).

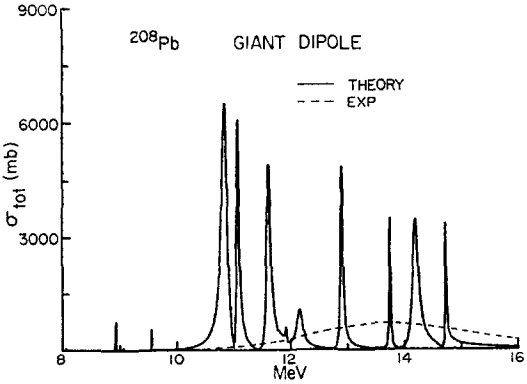

Fig. 10. Same as fig. 8 for ^{208}Pb. Experimental data are from ref. [17]).

enough so that one peak dominates. It is clear that the widths obtained in ^{40}Ca and ^{208}Pb are too small to fit the experimental data, implying that mixing with more complicated states must dominate in these heavier nuclei. Finally, we mention the kinetic sum rule [16]),

$$\sum_n |\langle 0| \sum_i e_i r_i Y^1 |n\rangle|^2 (E_n - E_0) = \frac{3h^2e^2}{8\pi m} \frac{NZ}{A}. \tag{12}$$

The total strength we obtain in TDA exceeds this by $\approx 40\,\%$, which is greater than experimentally seen [17]). It is of importance to note here that the appropriate values for the RPA model (which contains correlation) are smaller by $\approx 30\,\%$ than those of the TDA model.

The authors thank S. F. Tsai for assistance. The computations were done on the Cyclotron Laboratory Σ-7 computer.

Appendix

We wish to derive, with our method, the golden rule of perturbation theory,

$$\Gamma = 2\pi \sum_c |\langle r|V|c\rangle|^2 \rho_c . \tag{A.1}$$

Here $|r\rangle$ is the resonant state of the system, and $|c\rangle$ is a state with a particle in the continuum. The density of continuum states, ρ_c is given by

$$\rho_c = \frac{2}{\pi} \frac{m}{\hbar^2 k}, \tag{A.2}$$

when the continuum states are normalized by

$$u_c(r) \to \sin(kr+\delta), \qquad \text{as } r \to \infty. \tag{A.3}$$

In our model, resonances occur at the poles of $(1-vG^{(0)})^{-1}$. The continuum part of $G^{(0)}$ may be expressed as

$$G^{(0)} = \sum_{p,h} \phi_h \frac{u_p(iu_p+w_p)}{(\hbar^2/2m)k_p} \phi_h, \tag{A.4}$$

with u_p a real function satisfying the boundary condition (A.3), and w_p a real function satisfying a similar boundary condition with a cosine dependence on $(kr+\delta)$. We first construct the theory omitting the imaginary part of $G^{(0)}$. This will produce real resonances,

$$(1-v \operatorname{Re} G^{(0)})^{-1} \approx v(r) \frac{\rho_t(r)\rho_t(r')}{E_r - E}. \tag{A.5}$$

Here $\rho_t(r)$ is the transition density to excite the resonance and E_r is the resonance energy. We now include the imaginary part of $G^{(0)}$ using the operator formula

$$(A+B)^{-1} = A^{-1}(1+BA^{-1})^{-1}. \tag{A.6}$$

We find

$$(1-vG^{(0)})^{-1} = (1-v \operatorname{Re} G^{(0)})^{-1}[1-iv \operatorname{Im} G^{(0)}(1-v \operatorname{Re} G^{(0)})^{-1}]^{-1}. \tag{A.7}$$

Using (A.4) and (A.5) we find

$$[1-iv \operatorname{Im} G^{(0)}(1-v \operatorname{Re} G^{(0)})^{-1}]_{r''r'} = \delta(r''-r')$$
$$-i \sum_{p,h} \frac{(\int dr\, u_p(r)\phi_h(r)v(r)\rho_t(r))}{(\hbar^2/2m)k_p(E_r-E)} v(r')u_p(r')\phi_h(r')\rho_t(r''). \tag{A.8}$$

To invert the operator (A.8) we use the general formula for the inversion of an operator consisting of the unit operator plus a dyadic matrix

$$(1+|\xi\rangle \otimes \langle\eta|)^{-1} = 1 - |\xi\rangle \frac{1}{1+\langle\xi|\eta\rangle} \langle\eta|. \tag{A.9}$$

Applying this to (A.8) and inserting in (A.7) we find that the pole becomes

$$(1-vG^{(0)})^{-1} \approx v(r')\rho_t(r') \times \frac{1}{E_r - E - i\frac{2m}{\hbar^2}\sum_{p,h}\frac{1}{k_p}\left(\int \mathrm{d}r\, u_p(r)v(r)\rho_t(r)\phi_h(r)\right)^2}\rho_t(r''). \tag{A.10}$$

This displays the width in the desired Breit-Wigner form, and the imaginary part, $\frac{1}{2}i\Gamma$, is identical to the perturbative results, eq. (A.1).

References

1) K. Itoh, M. Oyamada and Y. Torizuka, Phys. Rev. **C2** (1970) 2181
2) M. Nagao and Y. Torizuka, Phys. Rev. Lett. **30** (1973) 1068
3) S. Hanna *et al.*, Phys. Rev. Lett. **32** (1974) 114
4) K. Snover *et al.*, Phys. Rev. Lett. **32** (1974) 317
5) M. B. Lewis and F. E. Bertrand, Nucl. Phys. **A196** (1972) 337
6) G. Bertsch, Phys. Rev. Lett. **31** (1973) 121;
   G. Bertsch and S. F. Tsai, Phys. Reports, to be published
7) P. Ring and J. Speth, Phys. Lett. **44B** (1973) 477;
   S. Krewald and J. Speth, Phys. Lett. **52B** (1974) 295
8) S. Krewald, J. Birkholz, A. Faessler and J. Speth, Phys. Rev. Lett. **33** (1974) 1386
9) J. Birkholz, Nucl. Phys. **A184** (1972) 385
10) C. Mahaux and H. A. Weidenmüller, *Shell model approach to nuclear reactions* (North-Holland, Amsterdam, 1969) p. 11;
    H. Sagan, *Boundary and eigenvalue problems in mathematical physics* (Wiley, New York, 1961) ch. 9
11) B. Buck and A. D. Hill, Nucl. Phys. **A95** (1967) 271
12) R. F. Barrett *et al.*, Rev. Mod. Phys. **45** (1973) 44, and references cited therein
13) I. Bloch *et al.*, Phys. Rev. **80** (1950) 553
14) D. Vautherin and D. Brink, Phys. Rev. **C5** (1972) 626
15) E. Hayward, *Photonuclear reactions*, NBS Monograph 118, August 1970
16) A. M. Lane, *Nuclear theory* (Benjamin, New York, 1964) p. 107
17) A. Veyssiere *et al.*, Nucl. Phys. **A159** (1970) 561
18) J. Ahrens *et al.*, *Photonuclear reactions and applications*, ed. Berman (US Atomic Energy Commission, Oak Ridge, 1973) p. 23